nature synthesis

Article

https://doi.org/10.1038/s44160-022-00224-z

Catenated covalent organic frameworks constructed from polyhedra

Received: 16 May 2022

Accepted: 8 December 2022

Published online: 16 January 2023

Check for updates

Tianqiong Ma[1,2,3], Yi Zhou[4,5], Christian S. Diercks[1,2,3], Junpyo Kwon[6,7], Felipe Gándara[8], Hao Lyu[1,2,3], Nikita Hanikel[1,2,3], Pilar Pena-Sánchez[8], Yuzhong Liu[1,2,3], Nicolas J. Diercks[1,2,3], Robert O. Ritchie[6,7,9], Davide M. Proserpio[10], Osamu Terasaki[4,5] & Omar M. Yaghi[1,2,3]

Although the synthetic chemistry leading to interlocking molecular [*n*] catenanes of organic polyhedra (*n* = 2–3) and rings (*n* = 2–130) is established, the analogous chemistry that pertains to infinite three-dimensional systems ([∞]catenane) remains undeveloped. We report a series of [∞] catenane covalent organic frameworks (termed catena-COFs). These were synthesized by linking 4,4′-(1,10-phenanthroline-2,9-diyl)dibenzaldehyde to either of tris-(4-aminophenyl)-amine, -methane or -methanol through imine condensation. These combinations give discrete adamantane-like polyhedra, catenated by virtue of the copper(I) ions templating a mutually embracing arrangement of PDBs (points-of-catenation), which ultimately results in infinite catena-COF-805, 806 and 807. The crystal structures of these COFs obtained from electron microscopy and X-ray diffraction were determined to be isoreticular and to adopt the **bor-y** structure type.

Synthetic molecular architectures in which polyhedra or rings are held together through mechanical interlocking rather than chemical bonding are referred to as [*n*]catenanes (*n* denotes the number of mechanically linked units)[1–6]. In such catenated molecules, the constituents can move freely within the confines of their mechanically linked counterpart without parting company. This interlocking provides for large-amplitude motion at the molecular level without the need to make or break chemical bonds and has thus enabled the development of molecular machines[7–11]. Facilitating dynamics through interlocking is also known in nature, in which, for example, the viral capsid of bacteriophage HK97 comprises catenated proteins that have the required structural flexibility for the passage of genomic material[12]. Thus, discrete interlocking molecules of increasing complexity have been synthesized, and include catenanes of interlocking rings[1–4] and cages[13–16], rotaxanes[17–19] and one-dimensional (1D) poly[*n*] catenanes[20,21] or Olympic gels[22,23]. In contrast, the chemistry of [∞] catenane frameworks is undeveloped: several metal–organic frameworks that contain interlocking are known[24–33]; however, their design remains elusive. The challenge of making such systems is further highlighted by the complete absence of organic [∞]catenane frameworks in which discrete organic molecular constituents are linked by mechanical interlocking. Here, we report a series of [∞]catenane covalent organic frameworks (COFs), termed catena-COF-805, 806 and 807, which are formed through the mechanical interlocking of discrete organic adamantane-like polyhedra. The crystal structures of the three catena-COFs were solved by a combination of transmission electron microscopy (TEM) techniques and powder X-ray crystallography. Based on their crystal structure and the average particle size,

[1]Department of Chemistry, University of California, Berkeley, CA, USA. [2]Kavli Energy NanoScience Institute, Berkeley, CA, USA. [3]Bakar Institute of Digital Materials for the Planet, Division of Computing, Data Science, and Society, University of California, Berkeley, CA, USA. [4]Center for High-Resolution Electron Microscopy (ChEM), School of Physical Science and Technology, ShanghaiTech University, Shanghai, People's Republic of China. [5]Shanghai Key Laboratory of High-Resolution Electron Microscopy, ShanghaiTech University, Shanghai, People's Republic of China. [6]Department of Mechanical Engineering, University of California, Berkeley, CA, USA. [7]Materials Science Division, Lawrence Berkeley National Laboratory, Berkeley, CA, USA. [8]Department of New Architectures in Materials Chemistry, Materials Science Institute of Madrid, Consejo Superior de Investigaciones Científicas, Madrid, Spain. [9]Department of Materials Science and Engineering, University of California, Berkeley, CA, USA. [10]Dipartimento di Chimica, Università degli studi di Milano, Milano, Italy. e-mail: yaghi@berkeley.edu

it was calculated that each individual COF crystal was composed of millions of interlocking organic polyhedra.

The design of an [∞]catenane framework commenced with the identification of a topology that can be formed from the interlocking of rings or polyhedra (Supplementary Section 1). We targeted the **bor** topology[34] in which 3- and 4-connected vertices are linked alternately to produce an infinite 3D arrangement. Reticulation of the tetrahedral Cu(I)-bis[4,4′-(1,10-phenanthroline-2,9-diyl)dibenzaldehyde]tetrafluoroborate ($[Cu(PDB)_2]BF_4$) (ref. [35]) with tritopic tris-(4-aminophenyl)amine (TAPA), tris-(4-aminophenyl)methane (TAPM) and tris-(4-aminophenyl)methanol (TAPMol) linkers yields catena-COF-805, 806 and 807, respectively, with an interlocking **bor-y** topology (the underlying **bor** topology, Fig. 1). In $[Cu(PDB)_2]BF_4$, the copper centres preorganize two PDB ligands in a mutually embracing manner, such that their appended aldehyde groups approximate a tetrahedral geometry to meet the interlocking requirement for adjacent adamantane-like polyhedra. The angles between the two aldehyde functionalities of each phenanthroline ligand and the angles between the amino functionalities of TAPA, TAPM or TAPMol are close to the target angles of an adamantane-like polyhedron (70.5° and 120°). The minor deviation of the angles can be compensated for by rotation of the imine bonds that connect the building units, as well as by an additional flexibility imparted by the central atoms (−N, −CH, −COH) of the three tritopic amine linkers. The PDB forms one of the six corners of the adamantane-like polyhedron, in which each polyhedron is interlocked with six adjacent polyhedra through the copper(I) templates, with the tetrafluoroborate anions (BF_4^-) occupying the void spaces in and between the polyhedra to maintain charge balance, which thus yields a 3D [∞]catenane (Fig. 2). As catena-COF-805, 806 and 807 have isoreticular structures, we present below the details that pertain to the exemplar compound catena-COF-805 and only discuss catena-COF-806 and 807 where the differences are notable. The detailed synthesis and analysis of the three compounds and the corresponding methods and data are disclosed in Methods and Supplementary Information.

Results and discussion

Synthesis and characterization of catena-COFs

Catena-COF-805 was synthesized by linking $[Cu(PDB)_2]BF_4$ (8.0 mg, 0.008 mmol) with TAPA (3.3 mg, 0.011 mmol) in a mixture of 1,4-dioxane and mesitylene (v/v = 1:1, 0.5 ml). Aqueous acetic acid (6 mol l^{-1}, 50 µl) was added as a catalyst and 4-bromoaniline (27.5 mg, 20 equiv.) was added as a monofunctional amine modulator[36]. The reaction was carried out in a sealed pyrex tube and heated at 150 °C for three days. The resulting precipitate was collected by centrifugation, washed with *N,N*-dimethylformamide (DMF) and tetrahydrofuran (THF), and then activated at 120 °C for 12 h to yield a reddish-brown solid (yield: 8.1 mg, 75.7%; Methods and Supplementary Section 2). Thermogravimetric analysis indicates that the solid has a high thermal stability up to 500 °C (Supplementary Fig. 3), in agreement with previous findings for imine COFs.

The formation of imine linkages in catena-COF-805 was confirmed by Fourier-transform infrared spectroscopy and solid-state NMR spectroscopy (Supplementary Sections 4 and 5). When compared with those of the linkers, that is, $[Cu(PDB)_2]BF_4$ and TAPA, the Fourier-transform infrared spectrum of the COF shows both attenuation of the C=O stretching vibration at ~1,693 cm^{-1} and of the N–H stretch around 3,300 and 3,400 cm^{-1} (Supplementary Figs. 4–6), which thus confirms conversion of the aldehyde and amine starting materials. Comparison of the ^{13}C cross-polarization magic-angle spinning NMR spectra of the linkers with that of catena-COF-805 confirmed that the COF product featured characteristic signals of, as expected, both starting building units (Supplementary Figs. 7–9). In addition, the signal that corresponds to the aldehyde carbon at ~192 ppm, as well as the signals of the carbon atoms adjacent to the amino group in TAPA at 116–118 ppm are strongly attenuated, which further corroborates imine condensation between the aldehyde and amine building units. Attempts to observe the formed imine bonds (HC=N, expected at 154–156 ppm) by ^{13}C cross-polarization magic-angle spinning spectroscopy were complicated by the fact that the $[Cu(PDB)_2]BF_4$ linker itself contains C=N bonds (~155 ppm). However, direct evidence for the formation of new imine bonds can be obtained by ^1H–^{13}C heteronuclear correlation spectroscopy as the imine bonds (HC=N) contain H, whereas the C=N functionality in PDB does not. Here, the overlaid 2D spectra (Supplementary Figs. 10–12) show that for catena-COF-805, a new ^1H–^{13}C correlation signal was observed at ~155 ppm of ^{13}C and ~9 ppm of ^1H. In contrast, no correlation signal was observed around these chemical shifts in the spectra of the $[Cu(PDB)_2]BF_4$ linker.

Structure determination of catena-COFs

Powder X-ray diffraction (PXRD), discussed further below, of catena-COF-805 indicated a highly crystalline phase with a diffraction pattern distinct from those of the corresponding linkers (Supplementary Figs. 13–17). Scanning electron microscopy images of this COF showed a polyhedron-shaped morphology with an average crystal size of ~500 nm (Supplementary Fig. 18). To determine the crystal structures of the three catena-COFs, a combination of TEM techniques and PXRD analysis was employed. First, 3D electron diffraction (ED)[37] datasets were collected to obtain the reconstructed 3D reciprocal lattices (Supplementary Figs. 19–21). Catena-COF-805 crystallized in an *F* cubic lattice with a unit cell parameter of $a = 56.8$ Å, whereas catena-COF-806 and 807 both crystallized in a *P* cubic lattice with nearly identical unit cell parameters of $a = 28.4$ Å and $a = 27.6$ Å, respectively.

This information can also be deduced from the corresponding selected area electron diffraction (SAED) patterns of the three catena-COFs (Fig. 3a–d, Fig. 4a–d and Supplementary Fig. 22). The SAED patterns of the three catena-COFs are similar along each direction, albeit with minor differences (Supplementary Fig. 22). After confirming that the interference from multiple scattering can be eliminated (Supplementary Fig. 23), the *d* spacing for d_{400} of catena-COF-805 was calculated to be like that for d_{200} of catena-COF-806 and 807, and some extra reflections of odd-number indices, such as the 113 series, were only observed for catena-COF-805. These facts are in good agreement with the twice larger lattice parameter *a* of catena-COF-805. Despite these differences, the SAED patterns of the three catena-COFs all showed the same $C_6 + C_4$ symmetry, which indicates related cubic lattices. This result is corroborated by the 3D ED data and is also in accordance with the targeted **bor-y**-based structures, which implies that the three catena-COFs have similar topologies with only minor structural differences.

A comparison of high-resolution transmission electron microscopy (HRTEM) images of the three catena-COFs (Fig. 3e–h, Fig. 4e–h and Supplementary Fig. 25) supported our analysis presented above. Despite the roughly similar images for the three catena-COFs along each direction, a remarkable difference can be observed along the [1$\bar{1}$0] direction (Figs. 3g and 4g, and Supplementary Fig. 25c,g,k), which highlights the structural variations that cause the unit-cell doubling of catena-COF-805 compared with the unit cells of catena-COF-806 and 807. Specifically, an alternating arrangement of rows with differently sized bright spots is observed in all three HRTEM images along the [1$\bar{1}$0] for all the catena-COFs. However, the bigger bright spots are aligned in a zigzag pattern as represented by yellow arrows in the micrograph of catena-COF-805 (Fig. 3g and Supplementary Fig. 25c), whereas for catena-COF-806 and 807, these spots are aligned in a straight line (yellow line in Fig. 4g and Supplementary Fig. 25g,k). When a Fourier filter was applied to the image of catena-COF-805 with some odd-number indices masked, the resulting HRTEM image became the same as that of catena-COF-806 (Supplementary Fig. 26), which addresses that these reflections of the odd-number indices in the SAED pattern and the variations in HRTEM image along [1$\bar{1}$0] can be critical to differentiate the structures.

https://doi.org/10.1038/s44160-022-00224-z

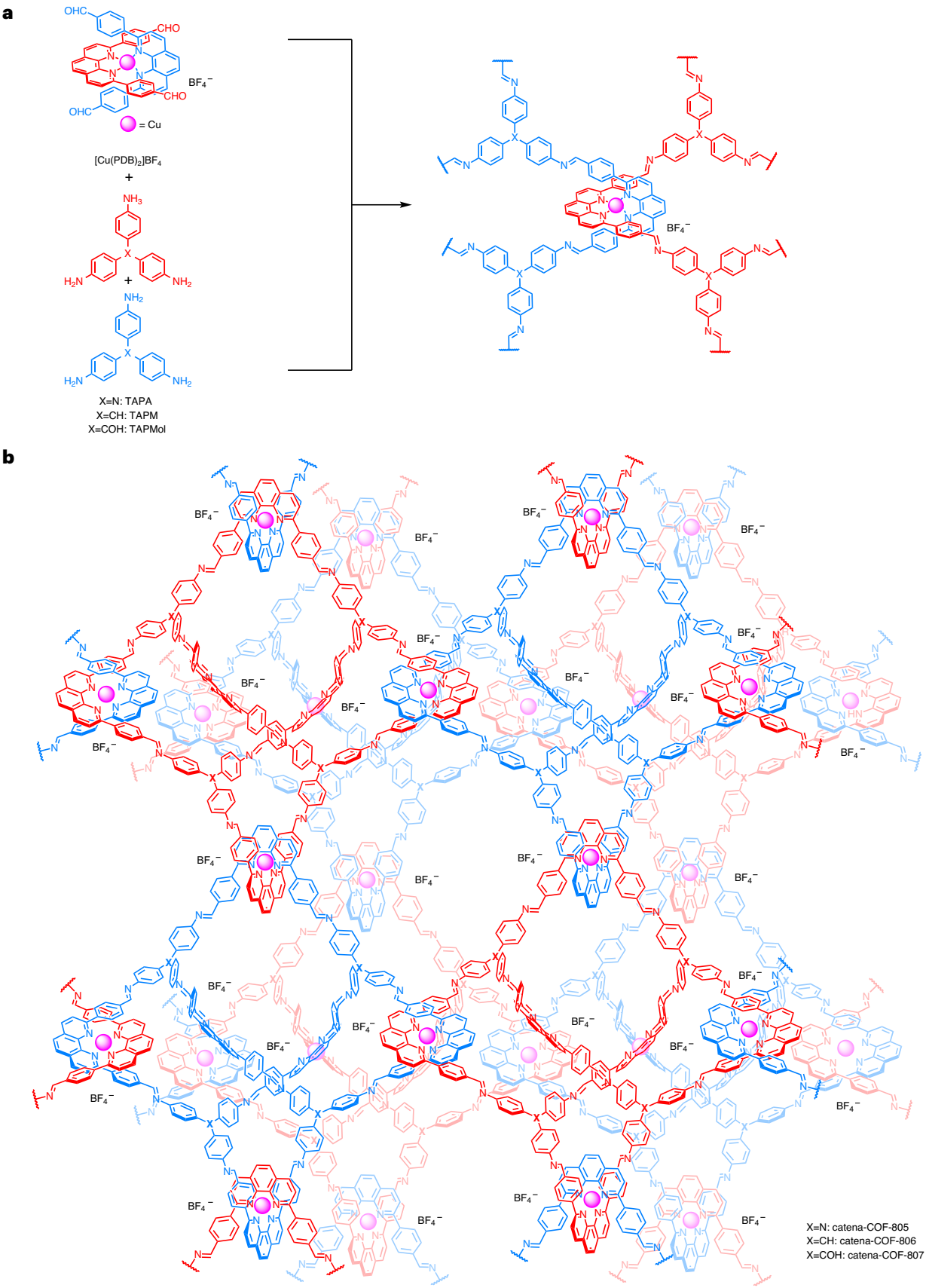

Fig. 1 | Synthetic strategy and design of the 3D [∞]catenane COFs. a,**b**, Catena-COF-805, 806 and 807 were synthesized by imine-formation reactions between tetrahedral $[Cu(PDB)_2]BF_4$ and tritopic TAPA, TAPM or TAPMol, respectively (**a**), to form extended structures of interlocking organic polyhedra with a Cu(I) template and BF_4^- as the counter anions (**b**). Two colours of red and blue are used to illustrate interlocking between each two polyhedra.

https://doi.org/10.1038/s44160-022-00224-z

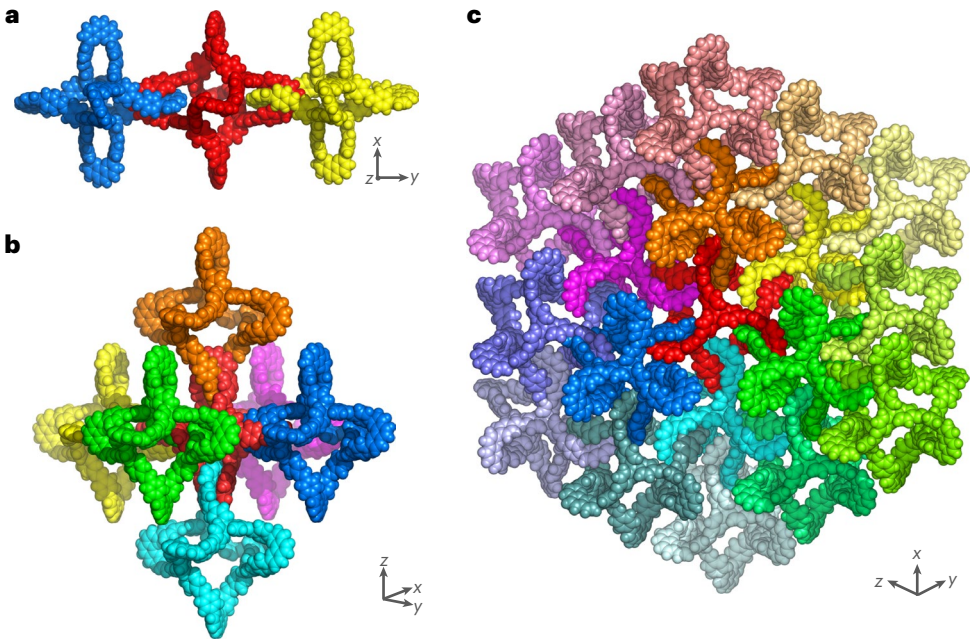

Fig. 2 | Perspectives of the crystal structure of catena-COF-805. The discrete polyhedra are represented by various colours. **a**, A fragment that contains three interlocking organic adamantane-like polyhedra in catena-COF-805. **b**, In the 3D [∞]catenane framework of catena-COF-805, each adamantane-like polyhedron is interlocked with six adjacent polyhedra through the Cu(I) templates, where each PDB serves as one of the six corners of a polyhedron, and the BF_4^- occupies the void spaces in and between the polyhedra for charge balance. Cu(I) ions and BF_4^- anions are omitted for clarity. **c**, The overall crystal structure of the extended framework constructed entirely of interlocking covalent polyhedra.

The datasets of each catena-COF were then integrated to be analysed for a structure solution (Fig. 3 for catena-COF-805, Fig. 4 for catena-COF-806 and Supplementary Fig. 27 for catena-COF-807). For catena-COF-805, the reflection conditions observed from the ED data (Fig. 3a–d and Supplementary Fig. 19) can be summarized as: *hkl*: $h + k$, $h + l$, $k + l = 2n$; 0*kl*: $k,l = 2n$; *hhl*: $h + l = 2n$; 00 *l*: $l = 4n$ (note that the weak abnormal reflections of the 002 series were proved to come from multiple scattering, see Supplementary Fig. 23), which suggests $F4_132$ (no. 210) as the only possible space group. An initial structure model of interlocking polyhedra with **bor-y** topology was built in $F4_132$ with the unit cell of $a = 56.8$ Å; however, projections of the model did not match with the HRTEM images (Supplementary Fig. 28). To account for these differences, a new model with a doubly interpenetrated **bor-y** topology (**bor-y-c***, Supplementary Fig. 29) was constructed. Comparison of the HRTEM images (Fig. 3e–h) with the projections of the interpenetrated model (Fig. 3i–l) yielded a perfect match along all directions. It is worth noting that the HRTEM information along the [1$\bar{1}$0] direction (Fig. 3g) aids in distinguishing unambiguously a non-interpenetrated from a doubly interpenetrated net (Supplementary Fig. 31). Accordingly, the overall reticular formula of catena-COF-805 was determined as $[(CuBF_4)_3(PDB)_6(TAPA)_4]_{imine}$, which matches well with the empirical formula of $C_{228}H_{144}N_{28}Cu_3B_3F_{12}$ and the elemental analysis (EA) result (Methods and Supplementary Section 2). All these results demonstrate that catena-COF-805 has a doubly interpenetrated **bor-y** structure.

Catena-COF-806 and 807 have the same *P* lattice and similar unit cell parameters of $a = 28.4$ Å and 27.6 Å, respectively. After elimination of the interference from multiple scattering (Supplementary Fig. 24), the only reflection rule that can be derived from the diffraction patterns of catena-COF-806 (Fig. 4a–d and Supplementary Fig. 20) and 807 (Supplementary Fig. 27a–d and Supplementary Fig. 21) is 00*l*: $l = 2n$, which yields the possible cubic space groups of $P4_232$ (no. 208) and $P2_13$ (no. 198). $P2_13$ can be excluded by deducing the plane group symmetries from HRTEM images and calculating the ratio of the vertices. For example, along the [1$\bar{1}$0] direction, the plane group *p*1*g*1 of $P2_13$ contains no mirror symmetry. However, the mirror symmetry is observed in the parallel alignment of arrays of bright spots in the HRTEM images of catena-COF-806 and 807 (Fig. 4g and Supplementary Fig. 27g). Indeed, the plane group of *p2mm* can be deduced, which is derived from space group $P4_232$, the only possible space group of catena-COF-806 and 807. This is in good agreement with the targeted **bor** type structure in which the ratio of 3-connected to 4-connected vertices is 4:3 after the symmetrical operation of $P4_232$. Structural models of the catena-COF-806 and 807 were constructed with the same doubly interpenetrated **bor-y** topology (**bor-y-c***, Supplementary Fig. 29) and the projections of the structure models for both catena-COF-806 (Fig. 4i–l) and 807 (Supplementary Fig. 27i–l) matched perfectly with the corresponding images from the HRTEM micrographs (Fig. 4e–h and Supplementary Fig. 27e–h). The reticular formulas of catena-COF-806 and 807 were then determined as $[(CuBF_4)_3(PDB)_6(TAPM)_4]_{imine}$ and $[(CuBF_4)_3(PDB)_6(TAPMol)_4]_{imine}$, respectively, which also match well with the empirical formulas of $C_{232}H_{148}N_{24}Cu_3B_3F_{12}$ for catena-COF-806 and $C_{232}H_{148}N_{24}O_4Cu_3B_3F_{12}$ for catena-COF-807. These results were further confirmed by EA (Methods and Supplementary Section 2).

PXRD refinements were carried out to confirm the structure models. Pawley refinement was conducted with the PXRD pattern of activated catena-COF-805 in the space group $F4_132$ (no. 210), which resulted in unit cell parameters of $a = 54.858(8)$ Å with $R_p = 0.63\%$ and $wR_p = 1.62\%$ (Fig. 5a). Similarly, the activated catena-COF-806 and 807 were both refined in the space group of $P4_232$ to yield unit cell parameters of $a = 27.854(4)$ Å for catena-COF-806 with $R_p = 0.69\%$ and $wR_p = 1.24\%$ (Fig. 5b), and $a = 26.1153(9)$ Å with $R_p = 0.45\%$ and $wR_p = 1.27\%$ for catena-COF-807 (Supplementary Fig. 32a). The structure models were then finalized by geometry optimization (Fig. 5c,d, Supplementary Fig. 32b and Supplementary Tables 1–3) and the simulated PXRD patterns from the structure models were found to be in good agreement with the experimentally obtained datasets (Supplementary Figs. 33–35).

Despite the same doubly interpenetrated **bor-y** topology, the structural difference in symmetry and unit cell size between

https://doi.org/10.1038/s44160-022-00224-z

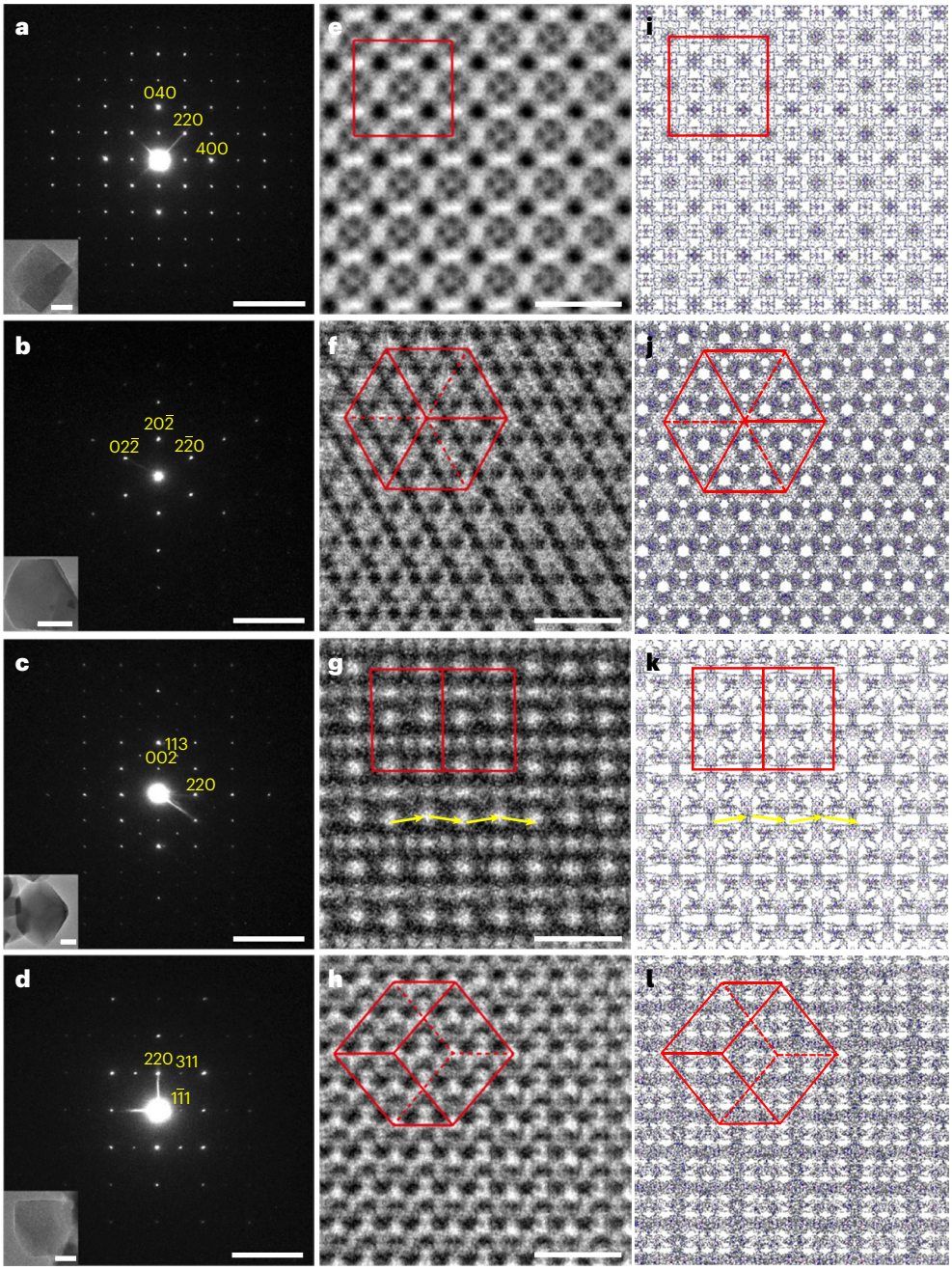

Fig. 3 | TEM data and perspective illustrations of the crystal structure of catena-COF-805. a–**d**, SAED patterns of catena-COF-805 from the [001] (**a**), [111] (**b**), [1$\bar{1}$0] (**c**) and [$\bar{1}$12] (**d**) incidences. Scale bars, 1 nm^{-1}. Insets: TEM images of the crystals used to collect data. Scale bars, 200 nm. **e**–**h**, HRTEM images of catena-COF-805 taken along the [001] (**e**), [111] (**f**), [1$\bar{1}$0] (**g**) and [$\bar{1}$12] (**h**) directions. Scale bars, 5 nm. **i**–**l**, Projections of the crystal structure of catena-COF-805 with a doubly interpenetrated **bor-y** topology along the [001] (**i**), [111] (**j**), [1$\bar{1}$0] (**k**) and [$\bar{1}$12] (**l**) directions. C, grey; N, blue; Cu, pink. H atoms and BF_4^- anions are omitted for clarity.

catena-COF-805 and 806 or 807 can be attributed to the various polyhedra orientations when they are interlocked with each other. Specifically, each two polyhedra in catena-COF-805 are interlocked by twisting 90° (for example, red and blue polyhedra, Fig. 5c), whereas they have an identical orientation both in catena-COF-806 and 807 (Fig. 5d and Supplementary Fig. 32b). When considering the difference in structure between the three catena-COFs, it is instructive to take a detailed look at geometric differences in their constituent polyhedral building units. Although an identical phenanthroline linker was used in synthesizing all three catena-COFs, the orientations of two respective phenanthroline units on opposite sides of the constituent polyhedra are approximately parallel to each other in the polyhedra of catena-COF-805 (Fig. 5e), but approximately orthogonal in the structures of catena-COF-806 and 807 (Fig. 5f and Supplementary Fig. 32). To accommodate the tetrahedral coordination of the Cu(I) template, two phenanthroline units of neighbouring polyhedra need to assume an orthogonal orientation to each other. Consequently, a rotation of alternating polyhedra is observed for catena-COF-805, in contrast to the lateral translation of neighbouring polyhedra in catena-COF-806 and 807. The differences in the structures of polyhedra are caused by the different geometries of their respective tritopic building blocks. Specifically, the N atoms at the centre of TAPA display a trigonal planar orientation of its aniline substituents

https://doi.org/10.1038/s44160-022-00224-z

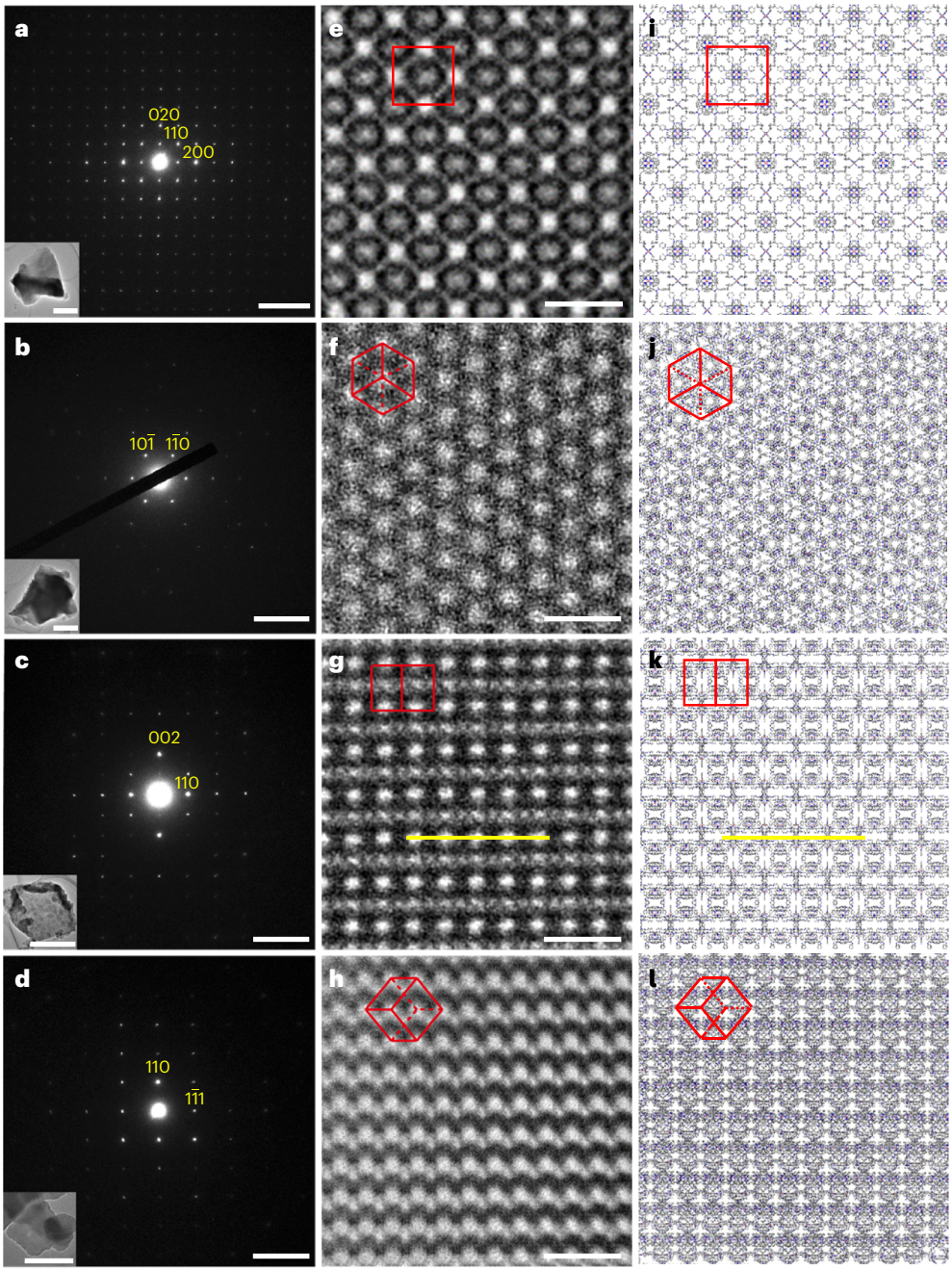

Fig. 4 | TEM data and perspective illustrations of the crystal structure of catena-COF-806. a–d, SAED patterns of catena-COF-806 from the [001] (**a**), [111] (**b**), [1 0] (**c**) and [12] (**d**) incidences. Scale bars, 1 nm^{-1}. Insets: TEM images of the crystals used to collect data. Scale bars, 200 nm. **e–h**, HRTEM images of catena-COF-806 taken along the [001] (**e**), [111] (**f**), [1$\bar{1}$0] (**g**) and [$\bar{1}$12] (**h**) directions. Scale bars, 5 nm. **i–l**, The projections of the crystal structure of catena-COF-806 with a doubly interpenetrated **bor-y** topology along the [001] (**i**), [111] (**j**), [1$\bar{1}$0] (**k**) and [$\bar{1}$12] (**l**) directions. C, grey; N, blue; Cu, pink. H atoms and BF_4^- anions are omitted for clarity.

(Fig. 5e). In contrast, these substituents are arranged in a trigonal pyramidal orientation in TAPM and TAPMol due to the tetrahedral geometry of their central C atoms (Fig. 5f and Supplementary Fig. 32). (Detailed angular values are displayed in Supplementary Fig. 36).)

Rietveld refinement and geometry optimization of crystal structures of catena-COF-806 and 807 (Supplementary Figs. 39 and 40 and Supplementary Table 1) yielded structures in which the C–H or C–OH bonds of the TAPM and TAPMol centres point towards the inside of their respective polyhedra (Supplementary Figs. 37 and 38), and thus yield polyhedra with a concave structure (Supplementary Fig. 38). Together, these structural differences account for the different polyhedron sizes of ~35.5 Å, ~35.4 Å and ~33.7 Å for catena-COF-805, 806 and 807, respectively (Supplementary Fig. 37), which represents one of the largest organic polyhedra (>30 Å) (refs. [15,16,38,39]). Taken together, these structural differences account for the variations observed in the HRTEM of the three catena-COFs (Supplementary Figs. 30 and 31). Note that due to the intrinsic flexibility of the interlocking polyhedra, all three catena-COFs show a dynamic response to solvents, as confirmed by the observed variations in their PXRD patterns on the addition or removal of solvents (Supplementary Section 9).

https://doi.org/10.1038/s44160-022-00224-z

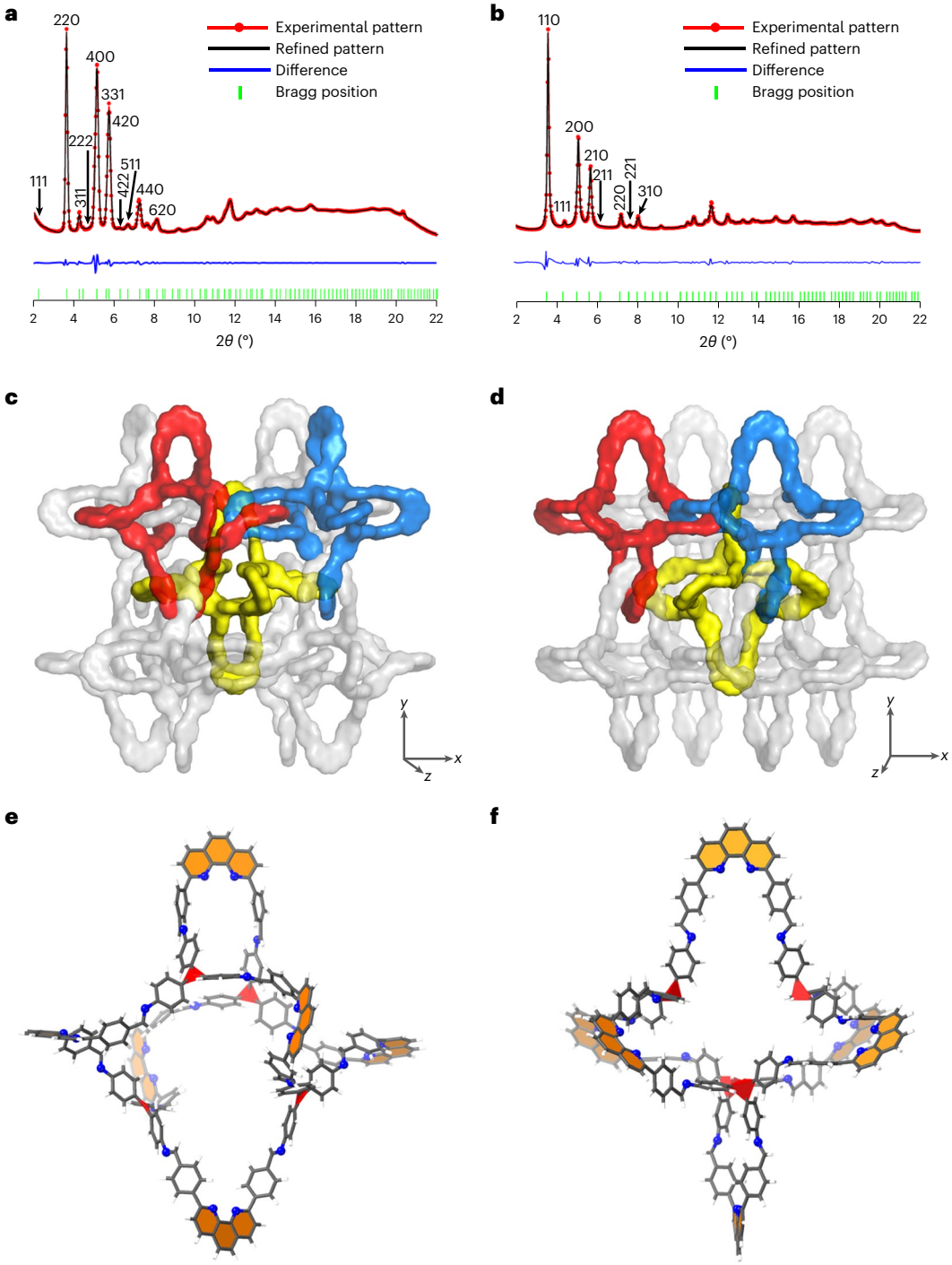

Fig. 5 | PXRD refinement and crystal structures of 3D [∞]catenane COFs. **a**,**b**, Pawley refinement of catena-COF-805 (**a**) and 806 (**b**) (λ = 1.2398 Å). **c**,**d**, The doubly interpenetrated **bor-y** frameworks of catena-COF-805 (**c**) and 806 (**d**) where their one subnet is represented by the catenated red, blue and grey polyhedra, and the other subnet is differentiated by representing it in yellow. In each subnet, every two catenated polyhedra (highlighted in red and blue) adopt different orientations in catena-COF-805, whereas all the polyhedra have the same orientations in catena-COF-806, which can be easily distinguished by the shape of the specific orientation of the polyhedra. **e**,**f**, The constituent polyhedron of catena-COF-805 (**e**) and 806 (**f**). The phenanthroline units (highlighted in orange) on opposite sides assume an approximately parallel orientation to each other in the polyhedron of catena-COF-805 (**e**), whereas they are oriented approximately orthogonal in that of catena-COF-806 (**f**). N atoms in the trifurcate centre of TAPA approach a planar triangle geometry (shown as a red triangle), whereas C atoms in the centre of TAPM adopt a tetrahedron geometry (shown as a red tetrahedron). C atoms, grey; N atoms, blue; H atoms, white.

Demetallation, flexibility and mechanical properties of catena-COFs

The crystal structures of catena-COFs were confirmed as the discrete adamantane-like polyhedra catenated by virtue of the copper(I) ions templating, so postsynthetic removal of the copper(I) ions was achieved up to 90% by the addition of aqueous KCN to yield the corresponding demetallated organic frameworks in which the covalent polyhedra are held together by mechanical bonds

(Supplementary Section 10). Although the non-crystalline structure of the demetallated catena-COFs (for example, demetallated catena-COF-806) cannot be directly verified by the crystallographic methods, its interlocking form was studied and discussed by control experiments (Supplementary Scheme 1 and Supplementary Figs. 48 and 49) and molecular dynamics simulation (Supplementary Fig. 53). We anticipated that the absence of copper(I) imparts a high degree of structural freedom onto the polyhedra. This was substantiated by the observed decrease in framework crystallinity on demetallation (Supplementary Fig. 51) and further by THF vapour sorption measurements (Supplementary Section 11). Here, catena-COF-806 exhibited a Type I THF adsorption isotherm with a characteristic micropore filling, whereas its demetallated derivative displayed a more linear THF isotherm profile (Supplementary Fig. 54). This indicates a structural expansion of demetallated catena-COF-806 and, indeed, a higher degree of flexibility, as borne out by the fact that the saturated uptake is doubled on demetallation.

The flexibility observed in the demetallated framework is manifested in the quasi-static and dynamic mechanical properties. The mechanical properties of both metallated and demetallated samples of catena-COF-806 were characterized by performing nanoindentation (Supplementary Section 12). The elastic modulus was found to decrease from 3.81 ± 0.60 GPa in metallated catena-COF-806 to 1.41 ± 0.37 GPa in the demetallated sample. The hardness decreases from 154.7 ± 27.7 MPa in the metallated catena-COF-806 to 55.8 ± 8.7 MPa after demetallation. All the measured values are within the expected range for weaving COFs[31]. The creep properties, measured as the change of the displacement under a constant load at room temperature, were studied to investigate the time-dependent plasticity of metallated and demetallated catena-COF-806. Maintaining compressive loads of 100 μN for 30 s yielded a creep depth of ~80 nm for the demetallated sample, compared with ~10 nm for its metallated analogue, which indicates that the demetallated catena-COF-806 is more mechanically flexible than the metallated sample.

Conclusions

In this work, a series of [∞]catenane COFs formed through mechanical interlocking of discrete organic adamantane-like polyhedra were synthesized and structurally characterized. We remark that obtaining [∞]catenane COFs crystals not only allows an unambiguous visualization of poly[*n*]catenane networks, but also affords a new method to assess the degree of catenation (*n*) by simply measuring the size of the crystals without sophisticated instrumental analysis, if one considers the crystal size obtained by scanning electron microscopy and the observed size of the unit cells (Supplementary Section 13). The previous record was held by an organic poly[*n*]catenane chain[21] with $n = 130$, whereas *n* in 3D catena-COFs is multiple orders of magnitude higher than the reported one, which highlights the prowess of reticular chemistry[40] in the design and synthesis of extended organic catenanes.

Methods

Synthesis of catena-COF-805

A pressure tube was charged with $[Cu(PDB)_2]BF_4$ (8.0 mg, 0.008 mmol), TAPA (3.3 mg, 0.011 mmol) and *p*-Br-aniline (27.5 mg, 20 equiv.) as a modulator. A mixture of 0.25 ml of 1,4-dioxane, 0.25 ml mesitylene and 0.05 ml of 6 M aqueous acetic acid was added. Then the tube was sealed and heated at 150 °C for 72 h to yield a reddish-brown solid at the bottom of the tube, which was isolated as catena-COF-805. The as-synthesized catena-COF-805 was washed with DMF and THF, and dried at room temperature for 12 h and at 120 °C for 12 h. This material is insoluble in water and in common organic solvents, such as methanol, acetone, THF, DMF and dimethylsulfoxide. Yield: 8.1 mg, 75.7%. EA results: calcd for $C_{228}H_{144}N_{28}Cu_3B_3F_{12}\cdot 20H_2O$: C 67.00%, H 4.50%, N 9.59%. Found: C 66.36%, H 4.22%, N 9.11%.

Synthesis of catena-COF-806

A pressure tube was charged with $[Cu(PDB)_2]BF_4$ (8.0 mg, 0.008 mmol) and TAPM (5.0 mg, 0.017 mmol). A mixture of 0.5 ml of 1,4-dioxane, 20 μl of aniline (24.4 equiv.) and 0.1 ml of aqueous acetic acid (6 M) was added and the tube was sealed. The reaction was heated at 120 °C for 72 h to yield a reddish-brown solid as catena-COF-806 at the bottom of the tube. The solid was isolated by centrifugation and washed with DMF and THF, and then dried at room temperature for 12 h and at 120 °C for 12 h. Similarly, this product is insoluble in water and in the common organic solvents mentioned for catena-COF-805. Yield: 7.6 mg, 71.0%. EA results: calcd for $C_{232}H_{148}N_{24}Cu_3B_3F_{12}\cdot 25H_2O$: C 68.13%, H 4.50%, N 7.91%. Found: C 68.93%, H 4.47%, N 8.09%.

Synthesis of catena-COF-807

A pressure tube was charged with $[Cu(PDB)_2]BF_4$ (8.0 mg, 0.008 mmol) and TAPMol (3.4 mg, 0.011 mmol). A mixture of 0.25 ml of 1,4-dioxane, 0.25 ml of mesitylene and 0.1 ml of aqueous acetic acid (6 M) was added and the tube was sealed. The reaction was heated at 85 °C for 72 h to yield a reddish-brown solid as catena-COF-807 at the bottom of the tube. The crude product was isolated by centrifugation and washed with DMF and THF, and then dried at room temperature for 12 h and at 120 °C for 12 h. Similarly, this product is also insoluble in water and in common organic solvents, as mentioned for catena-COF-805 and 806. Yield: 6.9 mg, 63.9%. EA results: calcd for $C_{232}H_{148}N_{24}O_4Cu_3B_3F_{12}\cdot 25H_2O$: C 69.17%, H 4.74%, N 8.01%. Found: C 69.58%, H 4.71%, N 7.93%. Note that all the obtained catena-COFs are air stable.

Transmission electron microscopy

Catena-COF samples for TEM analysis were dispersed in ethanol by ultrasonication. A droplet of the suspension was transferred onto a carbon-coated copper grid. All the datasets were obtained using a JEM-2100Plus microscope operated at 200 kV with a TVIPS (XF416) camera for high signal-to-noise ratio data acquisition. Owing to the beam sensitivity of the samples, 3D ED datasets were collected using a fast method in which the sample holder was tilted continuously and stopped every 5° for sample tracking. The obtained datasets were processed and reconstructed by the EDT-process program[37]. HRTEM images were obtained under low-dose conditions. Before taking images, the crystals were aligned to the desired orientations quickly under a depressed illumination condition. With a careful control of the electron dose and short exposure time, multiple images were taken and then integrated into one image to reduce the blur caused by sample drift.

Powder X-ray diffraction

The synchrotron PXRD datasets were collected at Beamline 7.3.3 of Advanced Light Source in the Lawrence Berkeley National Laboratory, with $\lambda = 1.2398$ Å in the capillary mode.

Data availability

Crystallographic data for the structures reported in this Article have been deposited at the Cambridge Crystallographic Data Centre, under deposition numbers CCDC 2216102 (catena-COF-805), 2216103 (catena-COF-806) and 2216104 (catena-COF-807). Copies of the data can be obtained free of charge via https://www.ccdc.cam.ac.uk/structures/. All data are available in the main text or the Supplementary Information.

References

1. Wasserman, E. The preparation of interlocking rings: a catenane. *J. Am. Chem. Soc.* **82**, 4433–4434 (1960).
2. Schill, G. & Lüttringhaus, A. The preparation of catena compounds by directed synthesis. *Angew. Chem. Int. Ed. Engl.* **3**, 546–547 (1964).
3. Dietrich-Buchecker, C. O., Sauvage, J.-P. & Kintzinger, J. P. Une nouvelle famille de molecules: les metallo-catenanes. *Tetrahedron Lett.* **24**, 5095–5098 (1983).

4. Ashton, P. R. et al. A [2] catenane made to order. *Angew. Chem. Int. Ed. Engl.* **28**, 1396–1399 (1989).
5. Forgan, R. S., Sauvage, J.-P. & Stoddart, J. F. Chemical topology: complex molecular knots, links, and entanglements. *Chem. Rev.* **111**, 5434–5464 (2011).
6. Gil-Ramírez, G., Leigh, D. A. & Stephens, A. J. Catenanes: fifty years of molecular links. *Angew. Chem. Int. Ed.* **54**, 6110–6150 (2015).
7. Sauvage, J.-P. et al. *Molecular Machines and Motors* (Springer, 2001).
8. Browne, W. R. & Feringa, B. L. Making molecular machines work. *Nat. Nanotechnol.* **1**, 25–35 (2006).
9. Kay, E. R., Leigh, D. A. & Zerbetto, F. Synthetic molecular motors and mechanical machines. *Angew. Chem. Int. Ed.* **46**, 72–191 (2007).
10. Stoddart, J. F. Mechanically interlocked molecules (MIMs)—molecular shuttles, switches, and machines. *Angew. Chem. Int. Ed.* **56**, 11094–11125 (2017).
11. Iino, R., Kinbara, K. & Bryant, Z. Introduction: molecular motors. *Chem. Rev.* **120**, 1–4 (2020).
12. Wikoff, W. R. et al. Topologically linked protein rings in the bacteriophage HK97 capsid. *Science* **289**, 2129–2133 (2000).
13. Fujita, M., Fujita, N., Ogura, K. & Yamaguchi, K. Spontaneous assembly of ten components into two interlocked, identical coordination cages. *Nature* **400**, 52–55 (1999).
14. Hasell, T. et al. Triply interlocked covalent organic cages. *Nat. Chem.* **2**, 750–755 (2010).
15. Zhang, G., Presly, O., White, F., Oppel, I. M. & Mastalerz, M. A shape-persistent quadruply interlocked giant cage catenane with two distinct pores in the solid state. *Angew. Chem. Int. Ed.* **53**, 5126–5130 (2014).
16. Benke, B. P., Kirschbaum, T., Graf, J., Gross, J. H. & Mastalerz, M. Dimeric and trimeric catenation of giant chiral [8+12] imine cubes driven by weak supramolecular interactions. *Nat. Chem.* (2022). https://doi.org/10.1038/s41557-022-01094-w
17. Harrison, I. T. & Harrison, S. Synthesis of a stable complex of a macrocycle and a threaded chain. *J. Am. Chem. Soc.* **89**, 5723–5724 (1967).
18. Anelli, P. L., Spencer, N. & Stoddart, J. F. A molecular shuttle. *J. Am. Chem. Soc.* **113**, 5131–5133 (1991).
19. Leigh, D. A., Wong, J. K. Y., Dehez, F. & Zerbetto, F. Unidirectional rotation in a mechanically interlocked molecular rotor. *Nature* **424**, 174–179 (2003).
20. Niu, Z. & Gibson, H. W. Polycatenanes. *Chem. Rev.* **109**, 6024–6046 (2009).
21. Wu, Q. et al. Poly[*n*]catenanes: synthesis of molecular interlocked chains. *Science* **358**, 1434–1439 (2017).
22. Raphael, E., Gay, C. & de Gennes, P. G. Progressive construction of a 'Olympic' gel. *J. Stat. Phys.* **89**, 111–118 (1997).
23. Fischer, J., Lang, M. & Sommer, J. U. The formation and structure of Olympic gels. *J. Chem. Phys.* **143**, 243114 (2015).
24. Jin, C.-M., Lu, H., Wu, L.-Y. & Huang, J. A new infinite inorganic [*n*] catenane from silver and bis(2-methylimidazoyl)methane ligand. *Chem. Commun.* **2006**, 5039–5041 (2006).
25. Loots, L. & Barbour, L. J. An infinite catenane self-assembled by *π*···*π* interactions. *Chem. Commun.* **49**, 671–673 (2013).
26. Thorp-Greenwood, F. L., Kulak, A. N. & Hardie, M. J. An infinite chainmail of M6L6 metallacycles featuring multiple Borromean links. *Nat. Chem.* **7**, 526–531 (2015).
27. Kuang, X. et al. Assembly of a metal–organic framework by sextuple intercatenation of discrete adamantane-like cages. *Nat. Chem.* **2**, 461–465 (2010).
28. Heine, J., Schmedt auf der Günne, J. & Dehnen, S. Formation of a strandlike polycatenane of icosahedral cages for reversible one-dimensional encapsulation of guests. *J. Am. Chem. Soc.* **133**, 10018–10021 (2011).
29. Jiang, L., Ju, P., Meng, X.-R., Kuang, X.-J. & Lu, T.-B. Constructions of two polycatenanes and one polypseudo-rotaxane by discrete tetrahedral cages and stool-like building units. *Sci. Rep.* **2**, 668 (2012).
30. Shen, Y., Zhu, H.-B., Hu, J. & Zhao, Y. Construction of a metal–organic framework by octuple intercatenation of discrete icosahedral coordination cages. *CrystEngComm* **17**, 2080–2082 (2015).
31. Chen, L., Chen, Q., Wu, M., Jiang, F. & Hong, M. Controllable coordination-driven self-assembly: from discrete metallocages to infinite cage-based frameworks. *Acc. Chem. Res.* **48**, 201–210 (2015).
32. Wu, X., Xu, Z.-X., Wang, F. & Zhang, J. Catenation of homochiral metal–organic nanocages or nanotubes. *Inorg. Chem.* **55**, 5095–5097 (2016).
33. Cheng, L. et al. Three-dimensional polycatenation of a uranium-based metal–organic cage: structural complexity and radiation detection. *J. Am. Chem. Soc.* **142**, 16218–16222 (2020).
34. O'Keeffe, M., Peskov, M. A., Ramsden, S. J. & Yaghi, O. M. The reticular chemistry structure resource (RCSR) database of, and symbols for, crystal nets. *Acc. Chem. Res.* **41**, 1782–1789 (2008).
35. Liu, Y. et al. Weaving of organic threads into a crystalline covalent organic framework. *Science* **351**, 365–369 (2016).
36. Ma, T. et al. Single-crystal X-ray diffraction structures of covalent organic frameworks. *Science* **361**, 48–52 (2018).
37. Gemmi, M. & Oleynikov, P. Scanning reciprocal space for solving unknown structures: energy filtered diffraction tomography and rotation diffraction tomography methods. *Z. Kristallogr.* **228**, 51–58 (2013).
38. Skowronek, P., Warżajtis, B., Rychlewska, U. & Gawroński, J. Self-assembly of a covalent organic cage with exceptionally large and symmetrical interior cavity: the role of entropy of symmetry. *Chem. Commun.* **49**, 2524–2526 (2013).
39. Ivanova, S. et al. Isoreticular crystallization of highly porous cubic covalent organic cage compounds. *Angew. Chem. Int. Ed.* **60**, 17455–17463 (2021).
40. Yaghi, O. M., Kalmutzki, M. J. & Diercks, C. S. *Introduction to Reticular Chemistry: Metal–Organic Frameworks and Covalent Organic Frameworks* (Wiley-VCH, 2019).

Acknowledgements

This research was partly supported by King Abdulaziz City for Science and Technology (Center of Excellence for Nanomaterials and Clean Energy Applications), and mechanical property measurements funded by the Defense Advanced Research Projects Agency (DARPA) under contract HR001-119-S-0048. This research used resources of the Advanced Light Source (beamline 7.3.3) at Lawrence Berkeley National Laboratory, which is a DOE Office of Science user facility under contract DE-AC02-05CH11231. Y.Z. and O.T. acknowledge the support of the Center for High-resolution Electron Microscopy (CħEM), ShanghaiTech University (EM02161943), Shanghai Science and Technology Plan (21DZ2260400) and National Natural Science Foundation of China (21835002). We thank C. Zhu for assistance in acquiring synchrotron PXRD data on beamline 7.3.3 of the Advanced Light Source, A. Lund and H. Celik of the School of Chemical Sciences at the University of California-Berkeley NMR facility for assistance with solid-state NMR data acquisition, Z. Wang at the Cornell High Energy Synchrotron Source and T. Matsumoto and A. Yamano at the Rigaku Co., Japan, for the initial trials on acquiring single-crystal XRD and PXRD data. D.M.P. thanks V. A. Blatov at the Samara Center for Theoretical Materials Science for providing the ToposPro software.

Author contributions

C.S.D., T.M. and O.M.Y. conceived the idea. T.M. and O.M.Y. led the project and interpreted the results. T.M. conducted the syntheses,

structure analyses and characterizations for all the samples and interpreted the data. Y.Z. and O.T. collected and analysed the TEM data, and supported the comparison of TEM and PXRD results. J.K. and R.O.R. collected and analysed the nanoindentation data. F.G. and P.P.S. finalized the PXRD refinement. H.L. and Y.Z. supported the scanning electron microscopy measurements. N.H. conducted the THF sorption experiment. Y.L. and N.J.D. supported the linker synthesis. D.M.P. helped in the literature and topological analysis of the organic polyhedra and catenation. T.M., C.S.D. and O.M.Y. wrote the manuscript and all the authors reviewed it.

Competing interests

The authors declare no competing interests.

Additional information

Supplementary information The online version contains supplementary material available at https://doi.org/10.1038/s44160-022-00224-z.

Correspondence and requests for materials should be addressed to Omar M. Yaghi.

Peer review information *Nature Synthesis* thanks the anonymous reviewers for their contribution to the peer review of this work. Primary Handling Editor: Alison Stoddart, in collaboration with the *Nature Synthesis* team.